JOURNAL OF MATERIALS SCIENCE 27 (1992) 6463–6474

Thermal stability of a platinum aluminide coating on nickel-based superalloys

H. M. TAWANCY, N. SRIDHAR, B. S. TAWABINI, N. M. ABBAS
Materials Characterization Laboratory, Research Institute, King Fahd University of Petroleum and Minerals, P. O. Box 1639, Dhahran 31261, Saudi Arabia

T. N. RHYS-JONES
Materials and Mechanical Research, Rolls-Royce plc, Bristol BS12 QE, UK

An investigation was carried out to determine the thermal stability of a platinum aluminide coating on the directionally solidified alloy MAR M 002 and its single-crystal version alloy, SRR 99, at 800, 1000 and 1100 °C. The morphology, structure and microchemical composition of the coating were characterized using scanning electron microscopy, transmission electron microscopy, energy dispersive X-ray spectroscopy and X-ray diffraction. In the as-deposited condition, the coating was found to consist of two layers. Most of the platinum was concentrated in the outer coating layer which consisted of a fine dispersion of $PtAl_2$ in a matrix of β-(Ni, Pt)Al containing other elements in solid solution, such as cobalt and chromium. The inner coating layer was relatively free of platinum and consisted essentially of β-NiAl. Exposure at 800 °C was found to have no significant effect on the structure and composition of the coating on each alloy. At temperatures $\geqslant$ 1000 °C, however, $PtAl_2$ became thermodynamically unstable and significant interdiffusion occurred between the coating and alloy substrate. After exposure at 1000 °C, the components of the outer coating layer were NiAl and Ni_3Al. However, after exposure at 1100 °C, the outer coating layer consisted only of Ni_3Al. Also, after exposure at both temperatures, the composition of the outer coating layer approached that of the inner layer due to interdiffusion. Although the coating on both alloys exhibited similar structural stability at all temperatures investigated, the coating on alloy MAR M 002 was found to develop a more protective scale. This behaviour was correlated with differences in alloy substrate composition particularly rare-earth elements such as hafnium.

1. Introduction

Aluminide coatings are commonly applied as standard surface protection systems for the γ′-strengthened nickel-based superalloys used in gas turbine blade applications [1]. It is the primary function of the coating to form a surface layer of β-NiAl after proper heat treatment [2]. During exposure to elevated temperatures, β-NiAl develops a protective scale based upon α-Al_2O_3.

One of the most significant modifications of aluminide coatings in order to improve their protective nature is the addition of platinum. In this case, the outer coating layer contains intermetallic phases such as $PtAl_2$, Pt_2Al_3 or PtAl depending upon the type of coating [3]. Currently, platinum aluminide coatings are used in certain applications and are likely to be more widely used in future gas turbine engines [4].

Earlier studies have demonstrated that platinum excludes refractory transition elements such as molybdenum, vanadium and tungsten from the outer coating layer which promotes selective oxidation of aluminium [5–7]. It is essential, however, that platinum remains concentrated in the outer coating layer.

Among the most important variables which can be expected to influence the performance capability of the coating is its thermal stability which refers to the influence of temperature on the structure and composition of the coating. During operation of a gas turbine engine, coated blades are exposed to an average temperature of about 1000 °C or slightly lower. However, due to hot spot conditions, the temperature may rise locally to about 1100 °C. At temperatures below about 1000 °C, interdiffusion between the coating and alloy substrate was suggested to play an insignificant role in coating degradation [8, 9]. In this case, oxide formation and spallation could play an important role [10]. At temperatures above 1000 °C, however, interdiffusion could be the most important variable influencing the performance capability of the coating [8, 9, 11].

It was the objective of this study to determine the thermal stability of a platinum aluminide coating on the directionally solidified alloy MAR M 002* and

* Registered trademark of Martin Marietta Corporation.

0022–2461

the single-crystal alloy SRR 99‡. Exposure temperatures below and above 1000 °C were selected for the study.

2. Experimental procedure

Table I summarizes the nominal chemical compositions of alloys MAR M 002 and SRR 99. Essentially, alloy SRR 99 is the single-crystal version of alloy MAR M 002 where grain-boundary strengthening elements such as carbon, boron and zirconium are eliminated. Rod-shaped specimens from both alloys (25 mm long and 8 mm diameter) were coated with a platinum aluminide of the RT§ 22LT-type which nominally contains 35%–55% Pt [12]. First, a layer of platinum was electroplated on the alloy surface. Following a diffusion treatment, the surface was aluminized in a high activity pack. The resulting coated alloys were then diffusion heat treated for 1 h at 1100 °C (argon). Finally, all the specimens were thermally aged for 16 h at 870 °C to precipitate the strengthening γ' phase.

To determine the effect of temperature on the structure and composition of the coating, as-coated specimens were exposed at 800, 1000 and 1100 °C for up to 900 h in air. Scanning electron microscopy (SEM) combined with energy dispersive spectroscopy (EDXS) and the transmission and scanning transmission electron microscopy (TEM/STEM) modes of an analytical electron microscope (AEM) equipped with an ultra-thin window X-ray detector and operating at 200 kV were used to characterize the microstructure and microchemical composition of the coating. The specimens were examined in the as-exposed condition to characterize the morphology and composition of surface scale. Prior to structural analysis of the outer coating layer by X-ray diffraction, the specimens were lightly polished to remove the surface oxide layer. To characterize the morphology and composition of the coating, cross-sections of the specimens were examined in the as-polished condition. Distinction between the different coating layers was made clearly visible by etching in Marble's reagent (10 g copper sulphate, 50 ml HCl, 50 ml H_2O). Also the microstructure of the alloy substrate was revealed by the same etchant. Thin-foil specimens from coating regions were prepared by the jet polishing technique in a solution consisting of 30% nitric acid in methanol at about − 20 °C. Structural analysis of outer coating layers was carried out using an X-ray diffractometer using CuK_α radiation.

TABLE I Nominal chemical composition (wt %) of alloys MAR M 002 and SRR 99

Element	Alloy MAR M 002	Alloy SRR 99
Ni	Bal.	Bal.
Cr	9	8.5
Al	5.5	5.5
Ti	1.5	2.2
Co	10	5
W	10	9.5
Ta	2.5	2.8
Hf	1.25	0.05[a]
Mo	0.5[a]	0.5[a]
Fe	0.5[a]	0.1[a]
Zr	0.055	0.01[a]
B	0.015	–
C	0.15	0.015

[a]Maximum.

‡ Registered trademark of Rolls-Royce plc.
§ Registered trademark of Chromalloy Gas Turbine Corporation.

3. Results and discussion

3.1. Microstructure of alloy substrates

In terms of the 100 h to rupture at 140 MPa, the temperature capability of alloy MAR M 002 is 1045 °C and that of alloy SRR 99 is 1080 °C [13]. Typical microstructures of the alloy substrates are illustrated in the secondary electron SEM images of Fig. 1. As expected, both alloys contained a fine dispersion of the γ' phase and larger globular γ', enriched in tungsten and tantalum. However, the density of the globular γ' was considerably less in the single-crystal alloy due to its higher melting range which permitted a more homogeneous structure to be produced [14]. Also, the directionally solidified alloy contained a greater density of primary MC-type carbide as can be expected. In addition, both alloys contained voids as shown in Fig. 1, which is typical of cast metal products.

Near the interdiffusion zone, the local chemical composition of both alloy substrates was comparable with the respective overall composition. Also, there was no evidence for alloy depletion.

3.2. Initial coating microstructure

In the as-deposited condition, the coating (~ 50 μm thick) was found to consist of two layers as illustrated in Fig. 2. Most of the platinum was concentrated in the outer layer (~ 25 μm thick) as demonstrated in Fig. 3. Analysis of X-ray diffraction data revealed that this layer consisted of a mixture of $PtAl_2$ (fcc, $a = 0.5926$ nm) and β-NiAl (B2-type superlattice, $a = 0.2887$ nm). A representative X-ray diffractometer trace derived from the outer coating layer and standard traces of $PtAl_2$ and NiAl are shown in Fig. 4a. Generally, the d-spacings of β-NiAl were slightly larger than expected of the pure phase. As demonstrated later, this could be due to the dissolution of platinum in β-NiAl. A corresponding X-ray spectrum representative of both alloy substrates is shown in Fig. 4b. In addition to the main three elemental constituents (nickel, platinum and aluminium), relatively small concentrations of chromium and cobalt were detected. For both alloy substrates, the outer coating layer was free of tungsten. Quantification of the spectral data of Fig. 4b (Table II) indicated that $PtAl_2$ was present as a secondary phase in a matrix of hyperstoichiometric β-NiAl (aluminium-rich) as expected of RT 22LT-type coating [12].

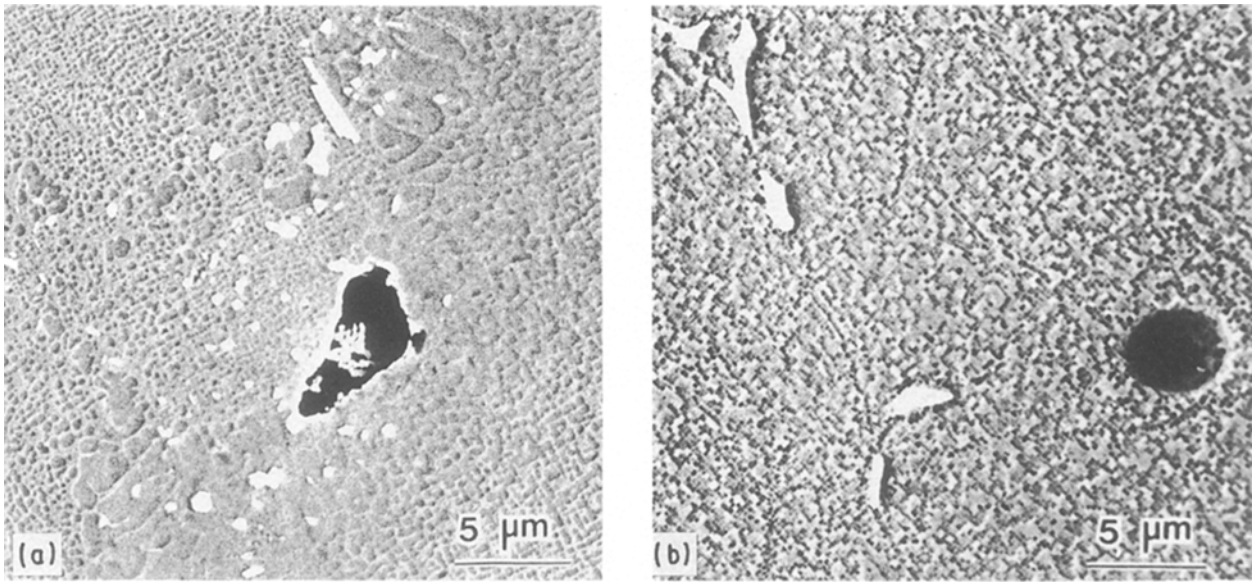

Figure 1 Secondary electron SEM images illustrating typical microstructures of the alloy substrates (etched). (a) Alloy MAR M 002. (b) Alloy SRR 99.

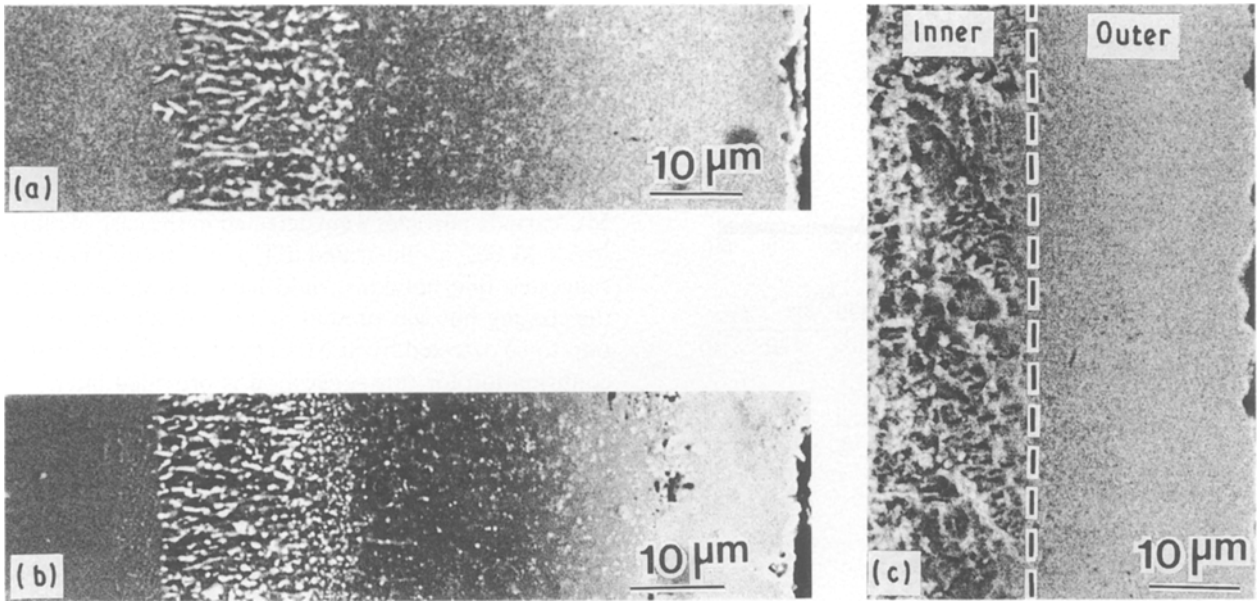

Figure 2 Secondary electron SEM images illustrating the morphology of platinum aluminide coating in the as-deposited condition. (a) Coating on alloy MAR M 002 (as-polished). (b) Coating on alloy SRR 99 (as-polished). (c) A representative example illustrating the two-layer coating structure (etched).

Although most of the platinum in the outer coating layer was present as $PtAl_2$, some appeared to partition to β-NiAl as suggested by the results of high-resolution lattice imaging. Fig. 5 illustrates a one-dimensional lattice fringe image of $(1\,1\,0)_\beta$ planes and the corresponding *d*-spacing profile in a region containing the inner and outer coating layers. In the inner coating layer, the *d*-spacing was more consistent with that of β-NiAl. However, as the outer coating layer was approached, the *d*-spacing gradually increased and then remained constant. It is possible to interpret this observation in terms of a gradual change in composition from β-phase relatively free of platinum in the inner coating layer into β-phase containing platinum in the outer coating layer. Most likely, vacancies in the nickel sublattice of the hyperstoichiometric β-phase in the outer coating layer were occupied by platinum to result in β-(Ni, Pt)Al of relatively larger *d*-spacings in comparison with β -NiAl (Fig. 4a).

As illustrated in the X-ray spectra of Fig. 6, the inner coating layer was relatively free of platinum in agreement with the results described above. It could be concluded from Fig. 6 and Table III that the inner coating layer consisted of hypostoichiometric β-NiAl (nickel-rich) with other elements in solid solution such as cobalt, chromium, titanium and tungsten.

A two-layer coating structure such as that shown in Fig. 2 evolves by outward diffusion of nickel [4, 6]. In this case, the outer coating layer consists of $PtAl_2$ dispersed in a matrix of hyperstoichiometric β-NiAl

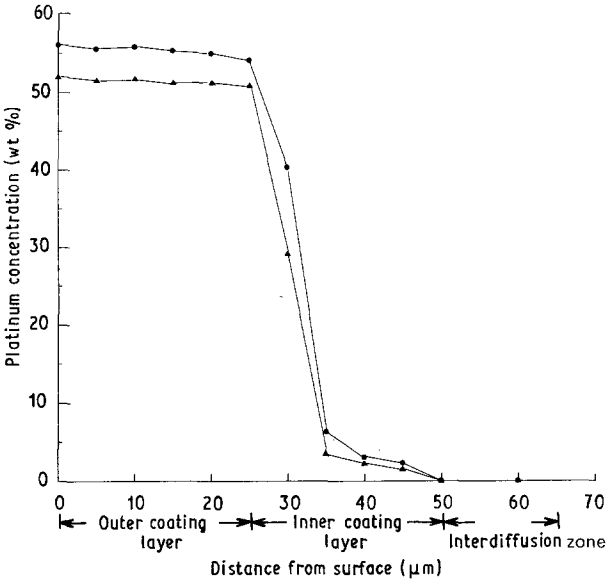

Figure 3 Concentration profile of platinum in the coating layer and interdiffusion zone in the as-deposited condition. (●) Alloy MAR M 002, (▲) alloy SRR 99.

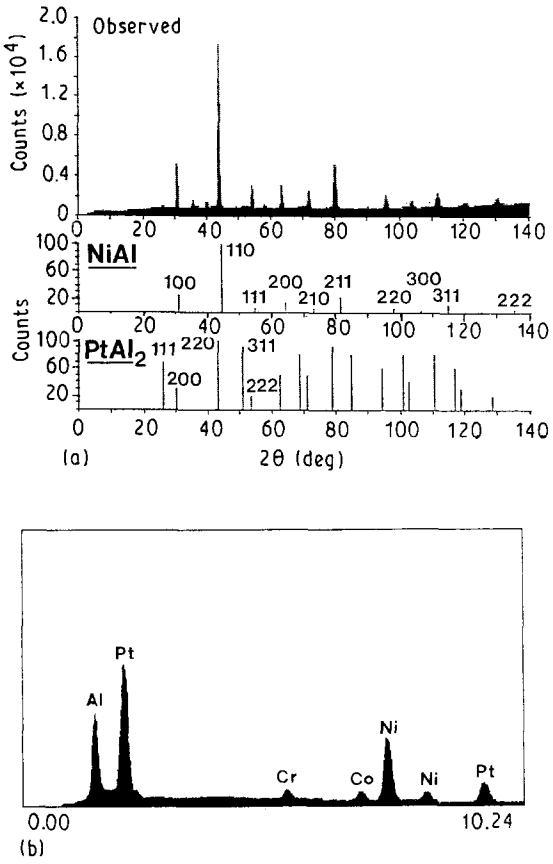

Figure 4 A representative example illustrating the structure and composition of the outer coating layer in the as-deposited condition. (a) X-ray diffractometer trace derived from the outer coating layer and standard traces of $PtAl_2$ and β-NiAl. (b) X-ray spectrum derived from the outer coating layer.

TABLE II Typical chemical composition (wt %) of the outer coating layer in the as-deposited condition

Pt	52.08
Al	13.51
Ni	28.10
Co	3.71
Cr	2.60

(aluminium-rich) and the inner layer consists of hypostoichiometric β-NiAl (nickel-rich) which forms by interdiffusion.

Fine precipitates observed in the inner coating layers (Fig. 2) were identified by TEM/STEM analysis to be predominantly of the α-Cr phase (b c c, $a = 0.2885$ nm). An example is given in Fig. 7. It could be concluded from the dark-field TEM experiment of Fig. 7a–c where the foil was oriented along $\langle 1\,1\,1\rangle_\beta$ direction that the characteristic reflections of the precipitates were overlapped with the fundamental b c c reflections of the β-phase. All *d*-spacings measured from the microdiffraction pattern of Fig. 7d were consistent with those of α-Cr. As demonstrated in the X-ray spectrum of Fig. 7e which was derived using an ultra-thin window detector that the main elemental constituent of the precipitates was chromium with trace amounts of molybdenum and nickel. Because the lattice constants of α-Cr and β-phase are almost identical, the above observations suggested that the two phases assumed a cube-to-cube orientation relationship.

Microchemical analysis by SEM/EDXS indicated that for both alloy substrates, the interdiffusion zone consisted of blocky particles of σ phase dispersed in a matrix of hypostoichiometric β-NiAl (nickel-rich) as can be expected [2]. An example is given in Fig. 8. As can be seen, that σ phase was of the type (Ni + Co)–Cr–W. Occasionally, however, hafnium-rich MC carbide particles were detected in the case of alloy MAR M 002, as illustrated in Fig. 9. This observation suggested that hafnium could have also diffused into the coating but was present in a too small concentration to be detected by SEM/EDXS (Fig. 4b). A further confirmation for this suggestion is provided later.

3.3. Structural stability of the coating

After 128 h exposure at 800 °C, the outer coating layer for both alloys still consisted of $PtAl_2$ and β-(Ni, Pt)Al similar to the case of the as-deposited condition described above. X-ray diffractometer traces derived

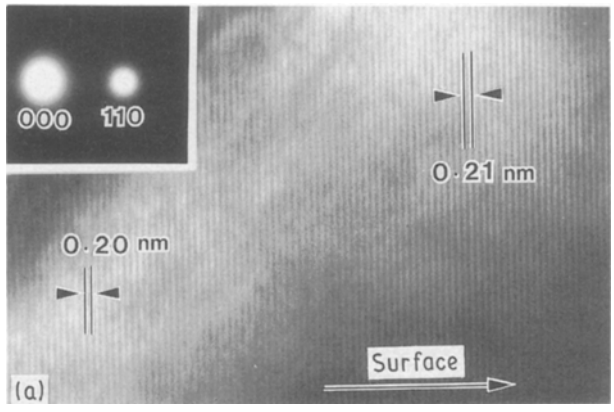

Figure 5 An example illustrating high-resolution TEM analysis of platinum aluminide coating in the as-deposited condition. (a) One-dimensional lattice fringe image of $(1\,1\,0)_\beta$ planes derived from a region containing the inner and outer coating layers. (b) Corresponding *d*-spacing profile.

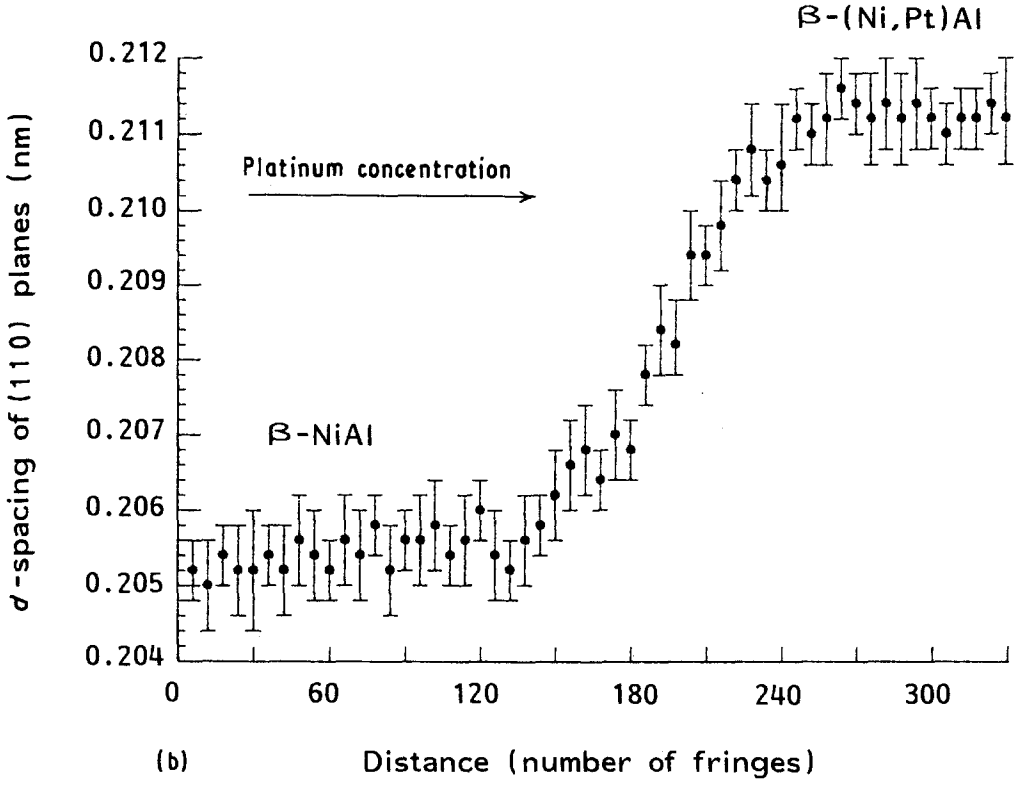

Figure 5 continued.

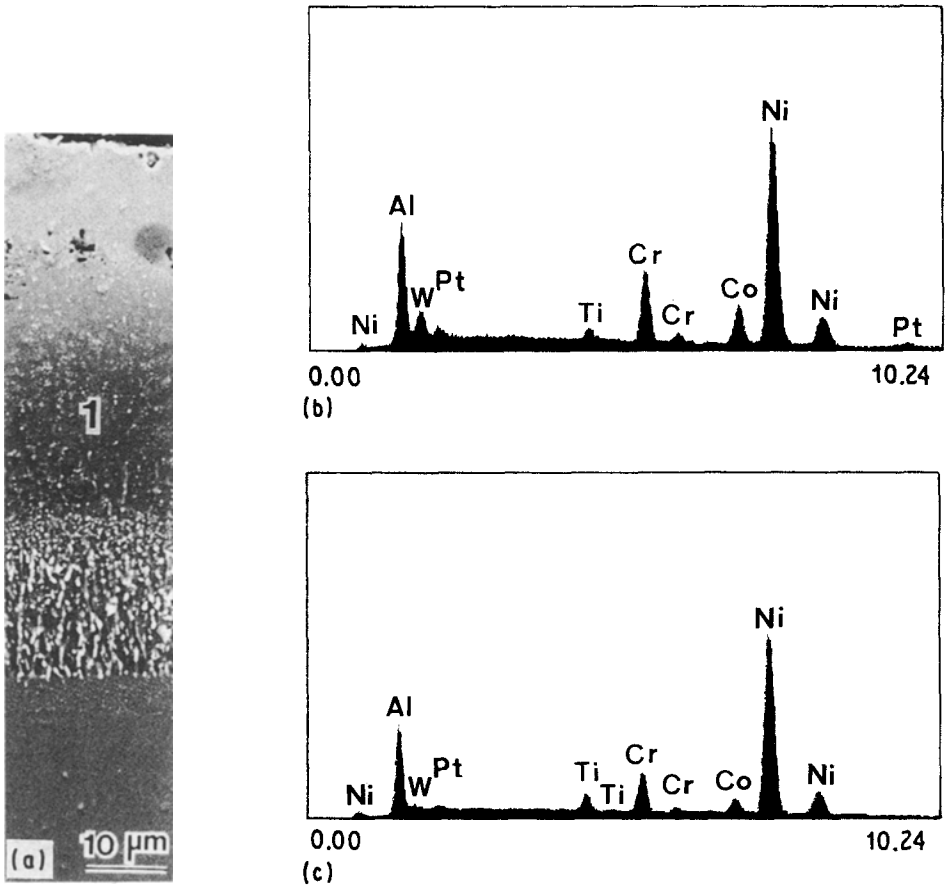

Figure 6 Chemical composition of the inner coating layer. (a) Representative secondary electron SEM image. (b) X-ray spectrum derived from the inner coating layer on alloy MAR M 002, region 1 in (a). (c) X-ray spectrum derived from the inner coating layer on alloy SRR 99, region 1 in (a).

from the outer coating layer were identical to that shown in Fig. 4a. Similar to the as-deposited condition, the coating still consisted of two distinct layers, as shown in Fig. 2.

In contrast to the above case, it was not possible to distinguish between the two coating layers after exposure at 1000 and 1100 °C. For example, Fig. 10 illustrates the effect of 500 h exposure at 1000 and 1100 °C on

TABLE III Chemical composition (wt %) of the inner coating layer in the as-deposited condition

Element	Alloy MAR M 002	Alloy SRR 99
Ni	58.19	67.25
Al	14.34	14.52
Pt	3.17	1.65
Co	9.71	5.08
Cr	5.03	7.08
Ti	1.38	2.38
W	8.18	2.03

the coating microstructure of alloy MAR M 002. A similar result was obtained in the case of alloy SRR 99. As the temperature was raised from 1000 °C to 1100 °C, the σ-phase particles in the interdiffusion zone were considerably coarsened and the zone itself became less clearly defined. After exposure at 1000 °C, precipitates were observed throughout the coating layer as shown in Fig. 10b. However, after exposure at 1100 °C (Fig. 10c), the coating layer was free of precipitates. Possibly, this behaviour could be related to both the structural changes described below and variation in coating composition illustrated in the next section.

Generally, after 100 h exposure at 1000 °C, $PtAl_2$ became thermodynamically unstable. As demonstrated in the representative X-ray diffractometer trace of Fig. 11a, the outer coating layer consisted of β-NiAl and γ′-Ni_3Al. However, β-NiAl appeared to be the major phase. After 100 h exposure at 1100 °C, the outer coating layer consisted only of γ′-Ni_3Al as shown in Fig. 11b. A further confirmation was provided by TEM/STEM analysis as illustrated in Fig. 12. Transformation of β-NiAl into γ′-Ni_3Al signified aluminium depletion from the coating. This would be expected to reduce the coating ability to develop and maintain a continuous Al_2O_3 protective scale.

Precipitates of the α-Cr phase present in the as-deposited condition were found to transform into σ-phase after exposure at 1000 °C. For example, Fig. 13 illustrates precipitates of the (Ni + Co)–Cr–W σ-phase in the coating layer of each alloy after 500 h exposure at 1000 °C.

It was possible to correlate the above structural changes with variations in coating composition caused by exposure to elevated temperatures, as described below.

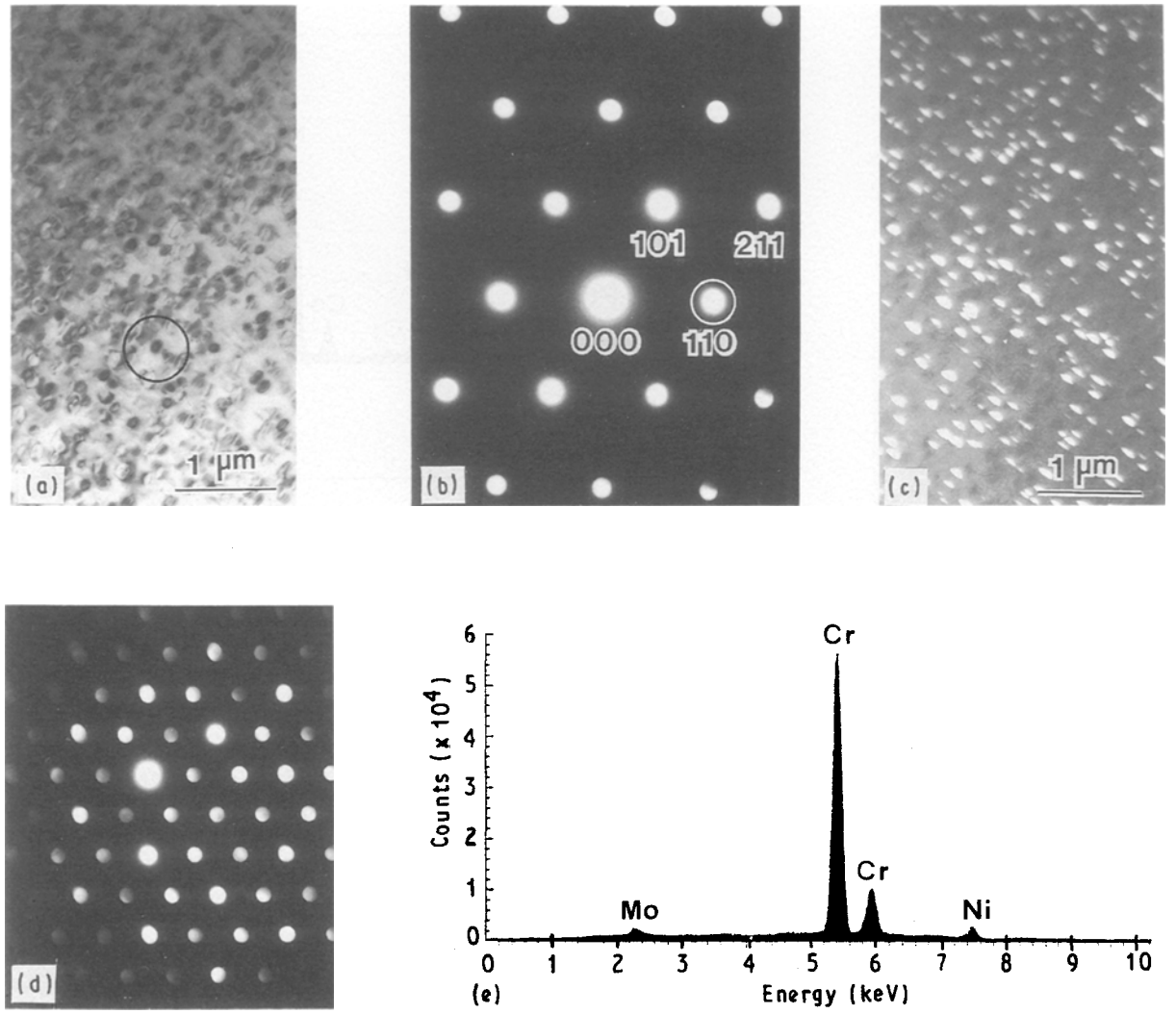

Figure 7 An example illustrating the identification of α-Cr precipitates in the inner layer of the coating (as-deposited condition). (a) Bright-field TEM image. (b) Corresponding selected-area diffraction pattern in $\langle 1\,1\,1\rangle_\beta$ orientation. (c) Dark-field image formed with the encircled $(1\,1\,0)_\beta$ reflection in (a). (d) $\langle 1\,1\,1\rangle$ microdiffraction pattern derived from the encircled α-Cr particle in (a) using the STEM mode. (e) X-ray spectrum derived from the same particle using STEM/EDXS with an ultra-thin window detector.

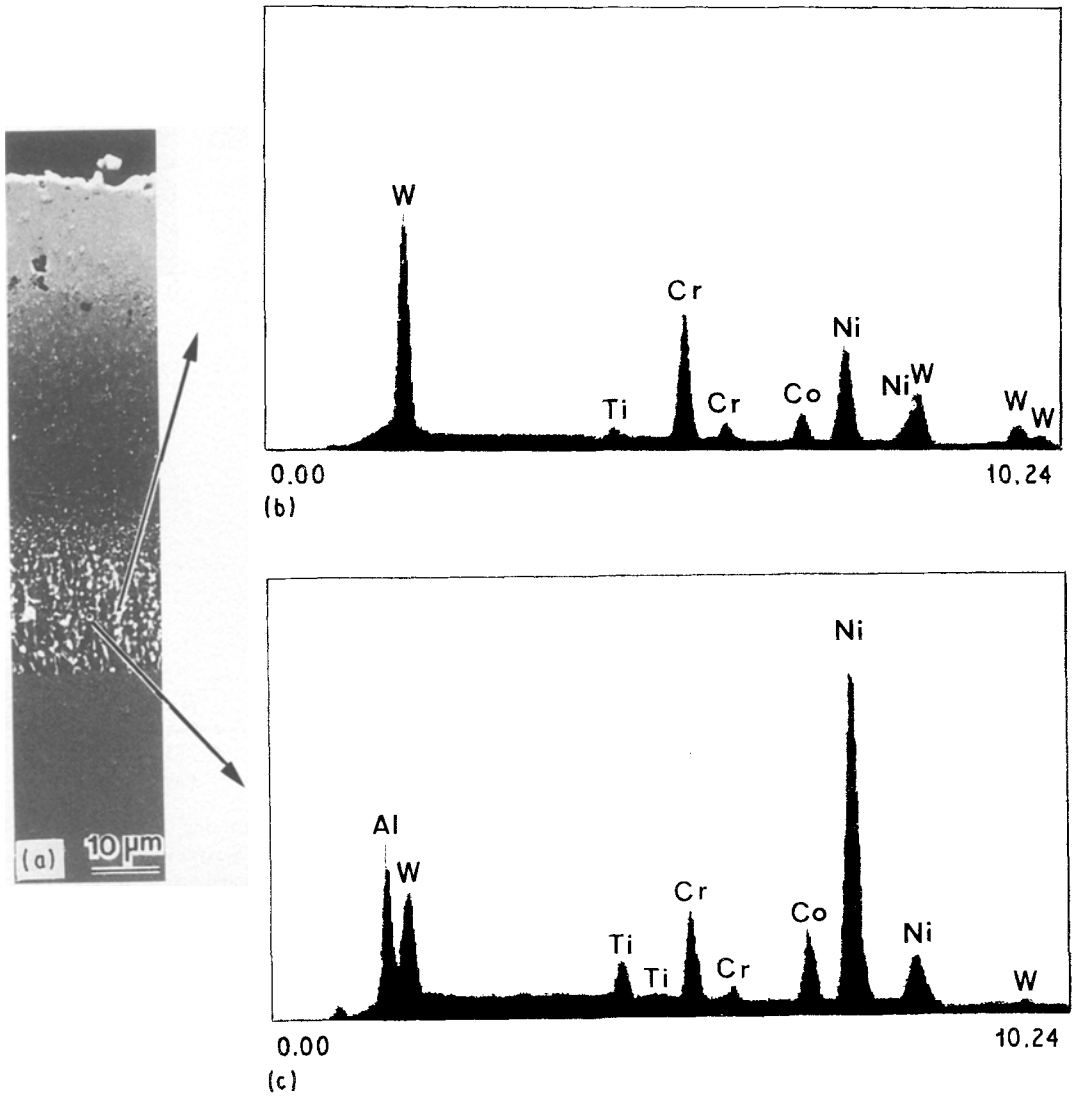

Figure 8 Constituents of the interdiffusion zone in the as-deposited condition. (a) Representative secondary electron SEM image. (b) X-ray spectrum derived from a σ-phase particle. (c) X-ray spectrum derived from the β-phase.

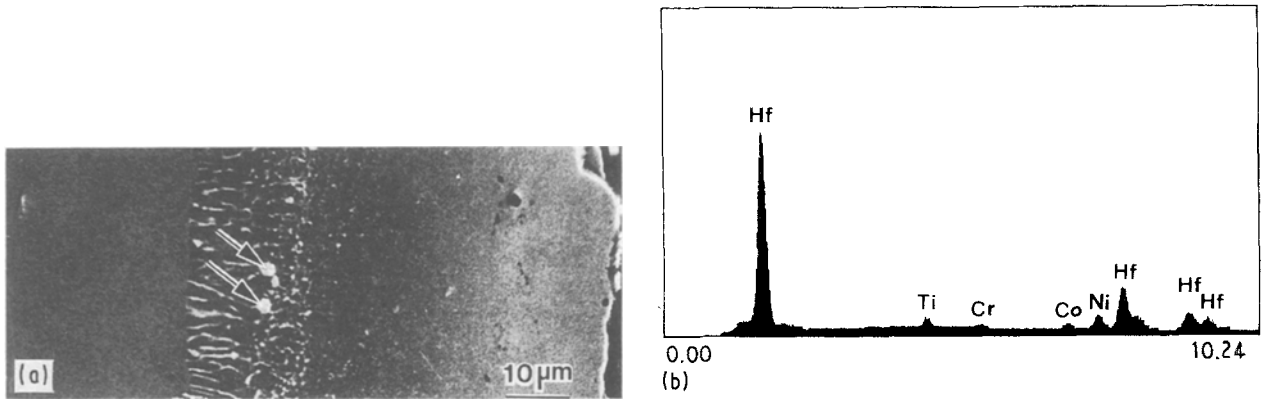

Figure 9 Identification of hafnium-rich MC carbide in the interdiffusion zone of alloy MAR M 002 (as-deposited condition). (a) Secondary electron SEM image; MC carbide particles are indicated by the arrows. (b) X-ray spectrum representative of the particles in (a).

3.4. Effect of temperature on coating composition

Exposure at 800 °C caused no significant change in coating composition as can be seen by comparing Figs 14 and 4b as well as the data of Table IV. It could be concluded from these results that there was no significant interdiffusion between the coating and substrate at 800 °C.

In contrast to the above case, after exposure at 1000 and 1100 °C, the composition of the outer coating layer approached that of the inner layer as demonstrated in the example of Table V which was derived from platinum aluminized alloy SRR 99. A similar result was obtained in the case of alloy MAR M 002. Fig. 15 illustrates the effect of exposure time at 1000 and 1100 °C on the platinum, aluminium and nickel

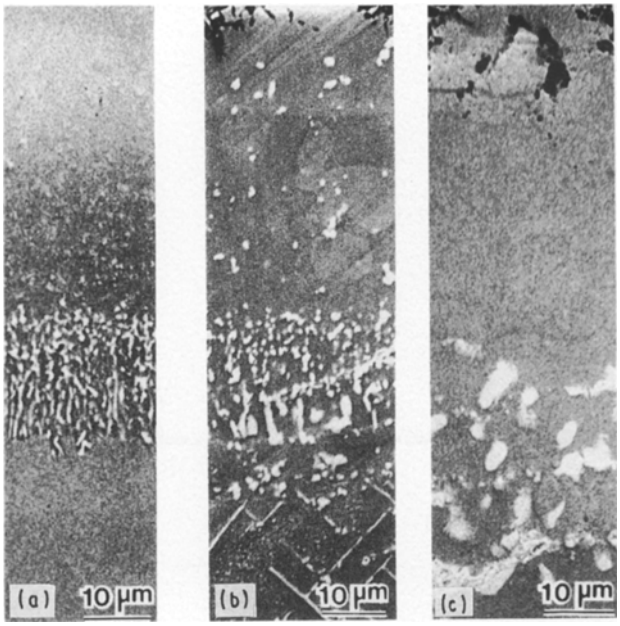

Figure 10 Secondary electron SEM images illustrating the effect of 500 h exposure at 1000 and 1100 °C on the coating microstructure of alloy MAR M 002. (a) As-deposited. (b) 500 h exposure at 1000 ° (c) 500 h exposure at 1100 °C.

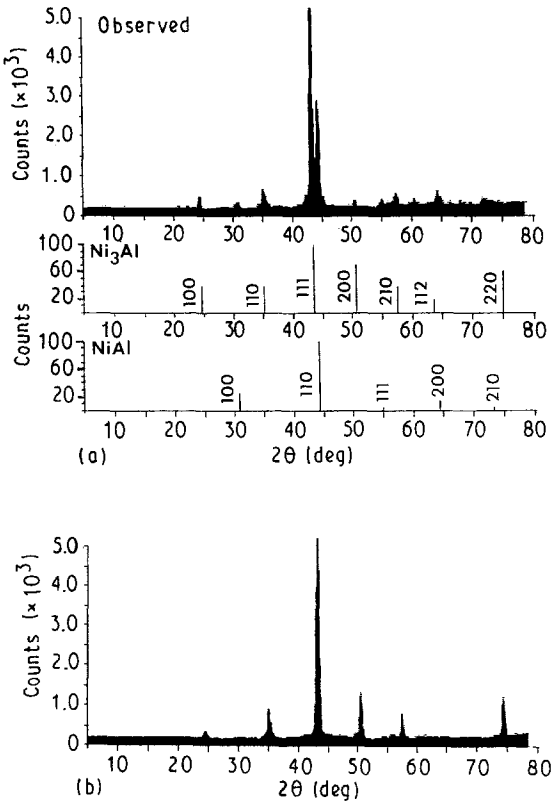

Figure 11 Effect of exposure at 1000 and 1100 °C on the structure of the outer coating layer. (a) X-ray diffractometer trace representative of the outer coating layer on each alloy after 100–900 h exposure at 1000 °C; standard traces of Ni_3Al and NiAl are shown. (b) X-ray diffractometer trace representative of the outer coating layer on each alloy after 100–900 h exposure at 1100 °C.

concentrations in the outer coating layer of each alloy. As can be seen, the platinum concentration was reduced from about 52–56 wt % in the as-deposited condition to less than 20 wt % after 100 h exposure at both temperatures. Subsequently, the platinum concentration remained essentially unchanged after up to 900 h exposure. In contrast, the aluminium concentration was only considerably reduced after 500 h exposure at both temperatures. Simultaneously, the nickel concentration in the outer coating layer was considerably increased after 100 h exposure at both temperatures and then remained nearly unchanged.

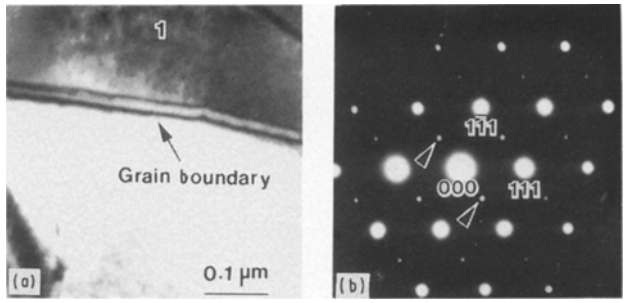

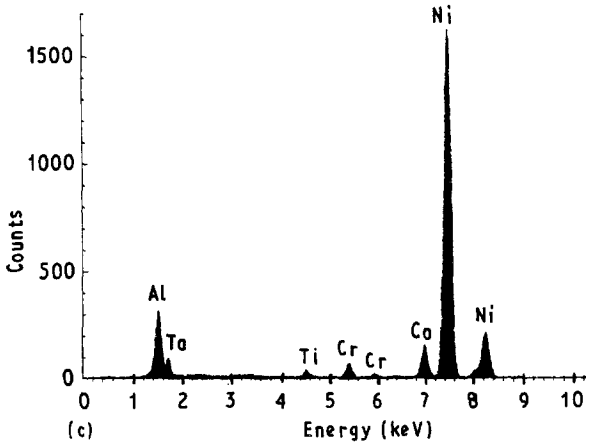

Figure 12 An example illustrating TEM/STEM analysis of the outer coating layer after 500 h exposure at 1100 °C. (a) Bright-field TEM image. (b) $[1\,0\,1]^-$ selected-area diffraction pattern from the grain marked 1 in (a); characteristic superlattice reflections of Ni_3Al are indicated by the arrows. (c) Corresponding X-ray spectrum.

Substantial reduction in the platinum concentration as shown in Fig. 15 could be attributed to the thermodynamic instability of $PtAl_2$ and inward diffusion of platinum. Although in the as-deposited condition the interdiffusion zone was virtually free of platinum, it contained about 15–18 wt % Pt after exposure at 1000 and 1100 °C, as shown in Fig. 16. Owing to the outward diffusion of nickel, the nickel to aluminium ratio was increased which favoured the formation of nickel-rich intermetallics such as Ni_3Al. However, due to the relatively higher aluminium concentration maintained after exposure at 1000 °C (Fig. 15), a mixture of NiAl and Ni_3Al was present as observed. Because of the additional decrease in aluminium concentration after exposure at 1100 °C, only Ni_3Al was present.

Another significant effect of exposure at 1000 and 1100 °C was the outward diffusion of both tungsten and chromium (σ phase-forming elements) as illustrated in the example of Fig. 17. This could explain the precipitation of σ phase in the coating layer. It is possible, however, that due to differences in the solubility of chromium and tungsten in NiAl and Ni_3Al, precipitates of the σ-phase were not present after

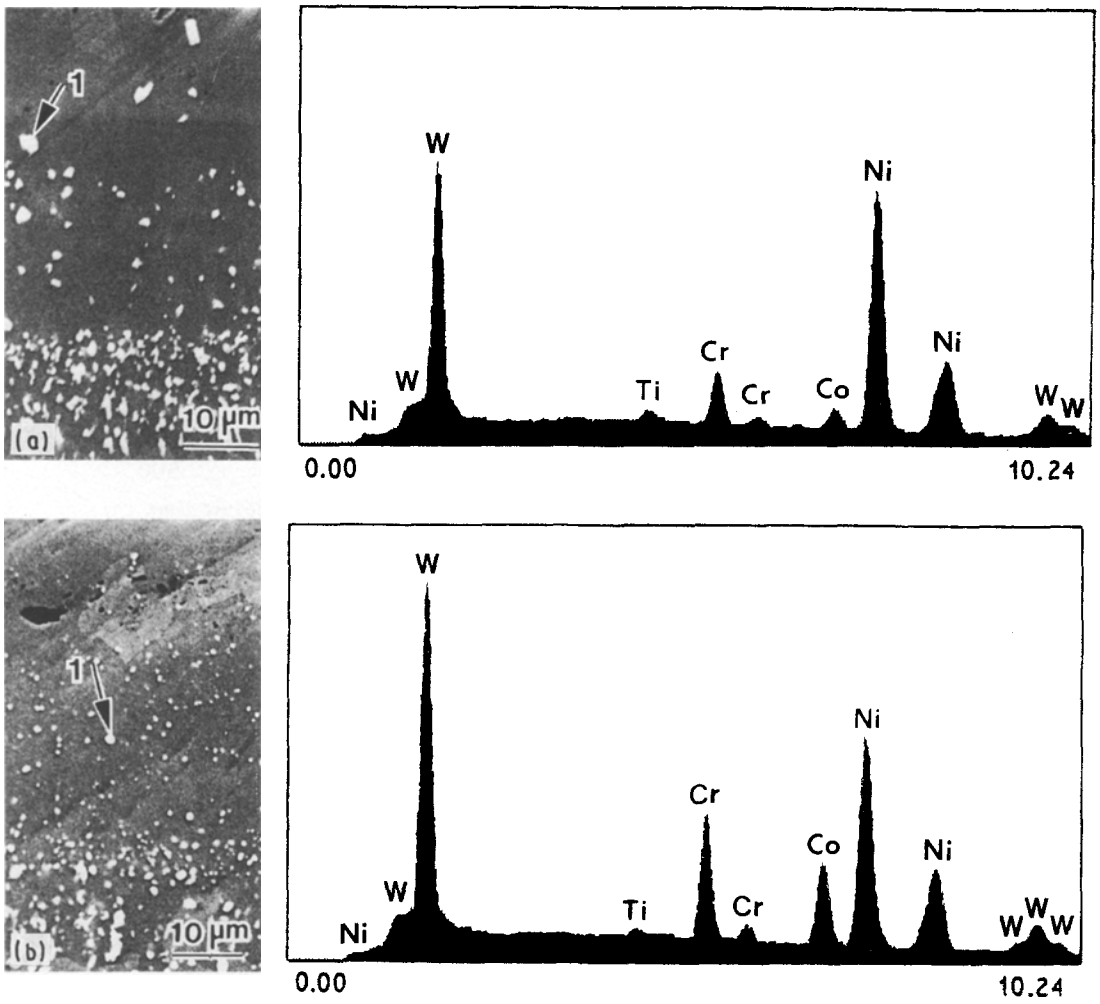

Figure 13 Identification of σ phase in the outer coating layer after 500 h exposure at 1000 °C. (a) Alloy MAR M 002; secondary electron SEM image and an X-ray spectrum derived from the precipitate particle marked 1. (b) Alloy SRR 99; secondary electron SEM image and an X-ray spectrum derived from the precipitate particle marked 1.

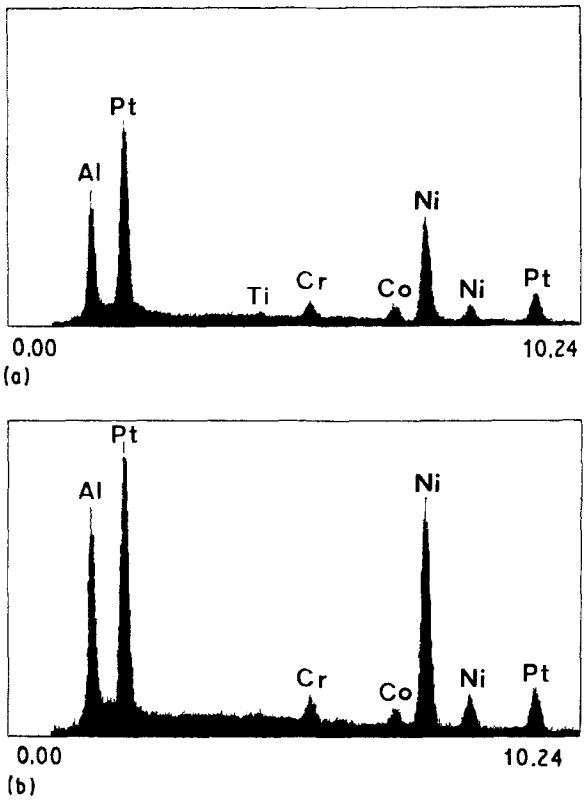

Figure 14 X-ray spectra derived from the outer coating layers after 128 h exposure at 800 °C. (a) Alloy MAR M 002. (b) Alloy SRR 99.

exposure at 1100 °C (Fig. 10c). Similar to the as-deposited condition, there was no evidence for significant alloy depletion near the interdiffusion zone.

Although the above results could suggest that the coatings on the two alloys develop similar oxide scales, this was not found to be the case as described below.

3.5. Influence of alloy substrate composition

As pointed out earlier, two variables can influence the performance capability of the coating: oxidation and interdiffusion. Because no significant interdiffusion occurred during exposure at 800 °C and the coating structure remained identical to that in the as-deposited condition, it could be concluded that isothermal oxidation did not have a significant effect on the structural stability of the coating below 1000 °C. However, both the morphology, structure and composition of surface scale developed by the coating on alloy MAR M 002 were different from those of alloy SRR 99. Fig. 18 illustrates the morphology of surface scale developed by the coating on each alloy after 128 h exposure at 800 °C in air. Microchemical analysis by EDXS and X-ray diffraction revealed that the scale of alloy MAR M 002 consisted of α-Al_2O_3 enriched in hafnium. In contrast, the scale of alloy

TABLE IV Effect of 128 h exposure at 800 °C on the chemical composition (wt %) of the outer coating layer

Element	Alloy MAR M 002		Alloy SRR 99	
	Unexposed	Exposed	Unexposed	Exposed
Pt	52.08	51.39	51.83	43.25
Al	13.51	12.69	13.51	13.61
Ni	28.10	29.48	31.86	38.09
Co	3.71	3.79	1.88	2.56
Cr	2.60	2.45	0.92	2.20
Ti	–	0.20	–	0.30
W	–	–	–	–

TABLE V Chemical composition (wt %) of the outer and inner coating layers of alloy SRR 99 after 100 h exposure at 1000 and 1100 °C

Element	100 h/1000 °C		100 h/1000 °C	
	Outer	Inner	Outer	Inner
Ni	60.32	59.66	61.23	61.08
Al	11.50	11.83	10.88	10.69
Pt	15.09	13.69	13.64	13.79
Co	4.47	4.55	4.20	4.39
Cr	5.66	5.70	7.09	7.35
Ti	1.58	1.69	1.15	1.21
W	1.37	2.87	1.81	1.49

SRR 99 consisted of granular particles of α-Al_2O_3 and an underlying $Ni(Al, Cr)_2O_4$ spinel. Reference to Table I indicates that alloy MAR M 002 contains 1.25 wt % Hf while alloy SRR 99 is free of hafnium. Because no interdiffusion occurred during exposure at 800 °C, it is likely that hafnium had diffused into the coating of alloy MAR M 002 during its application as indicated earlier.

Also, during exposure at 1000 and 1100 °C, where significant interdiffusion occurred, the scale developed by the coating on alloy MAR M 002 was different from that developed by the coating on alloy SRR 99 as illustrated in Fig. 19. In the case of alloy MAR M 002, the scale was found to consist of granular particles of α-Al_2O_3 and an underlying scale consisting of hafnium-rich Al_2O_3. It is to be noted that rare-earth elements such as hafnium and yttrium are known to stabilize other polymorphic forms of Al_2O_3 such as the ξ-phase [15]. Similar to exposure at 800 °C, the coating on alloy SRR 99 developed a scale consisting of granular particles of α-Al_2O_3 and an underlying less protective $Ni(Al, Cr)_2O_4$ spinel. As shown in Fig. 19, the scale of alloy MAR M 002 maintained a considerably finer structure in comparison with that of alloy SRR 99. Another possible beneficial effect of rare-earth elements such as hafnium and yttrium is to maintain a scale of fine-grained structure. For example, yttrium was found to segregate to grain boundaries of Al_2O_3 which could improve its elevated-temperature mechanical strength [16].

Based upon the above results, it could be concluded that although the coating on each alloy had similar thermal stability at the temperatures investigated, the scale developed by the coating on alloy MAR M 002

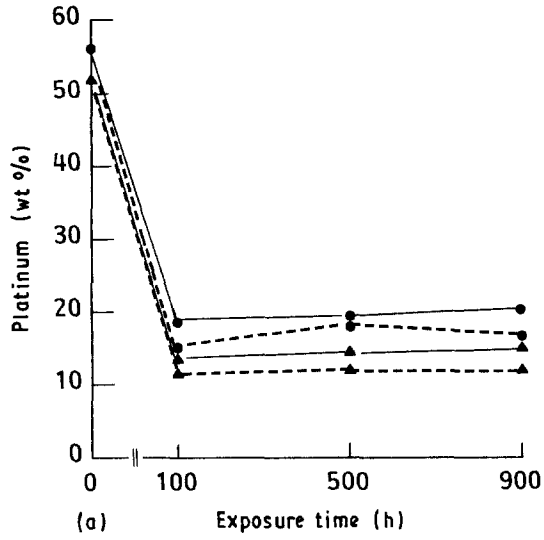

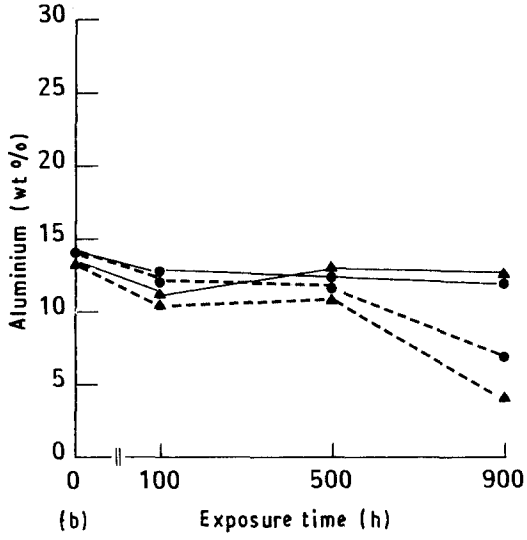

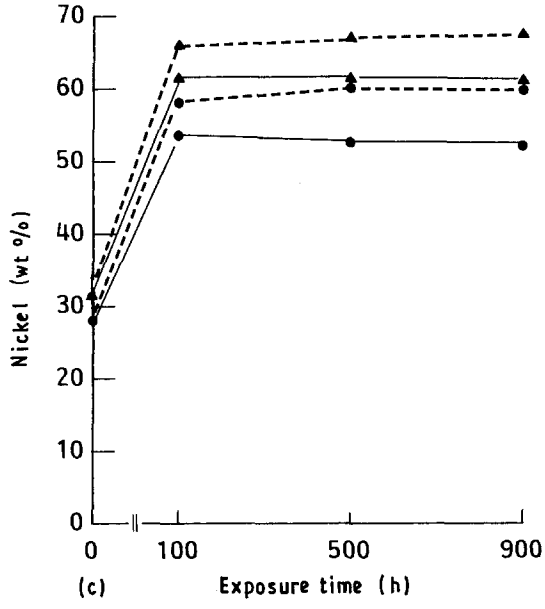

Figure 15 Effect of exposure time at (———) 1000 and (– – –) 1100 °C on the concentrations of (a) platinum (b) aluminium and (c) nickel in the outer coating layer, for (●) alloy MAR M 002 and (▲) alloy SRR 99.

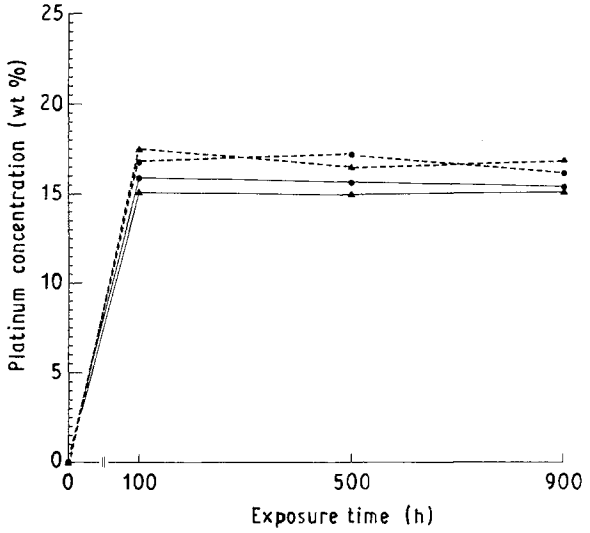

Figure 16 Effect of exposure time at (———) 1000 and (– – –) 1100 °C on the platinum concentration in the interdiffusion zone in (●) alloy MAR M 002 and (▲) alloy SRR 99.

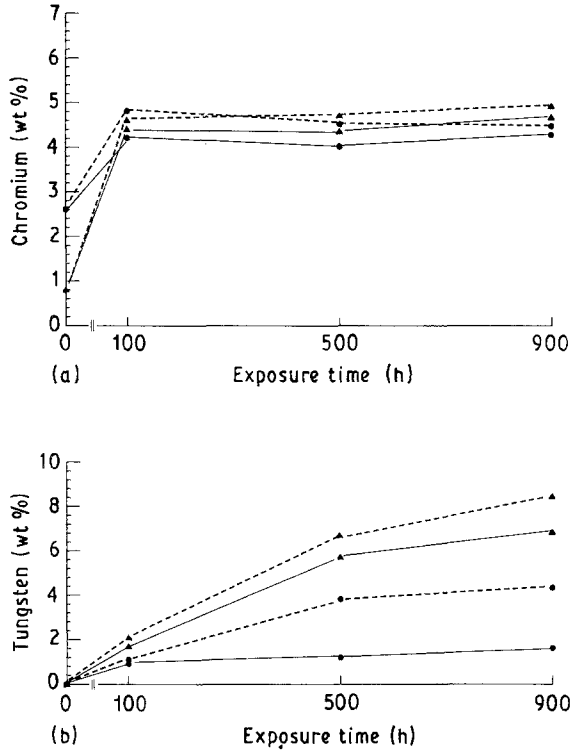

Figure 17 Effect of exposure time at (———) 1000 and (– – –) 1100 °C on the concentration of (a) chromium and (b) tungsten in the outer coating layer for (●) alloy MAR M 002, and (▲) alloy SRR 99.

would be more protective in comparison with that of alloy SRR 99. This behaviour could be related to differences in alloy substrate composition particularly rare-earth elements such as hafnium.

4. Conclusion

A study was conducted to examine the thermal stability of a platinum aluminide coating which evolves by

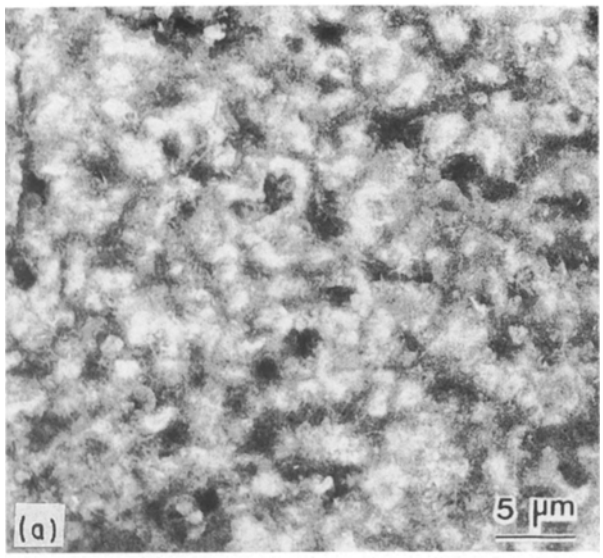

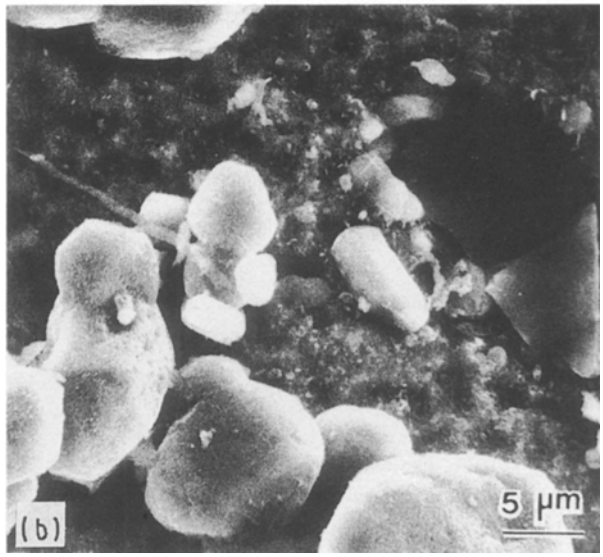

Figure 18 Secondary electron SEM images illustrating the morphology of surface scale developed by the coating on alloys (a) MAR M 002 and (b) SRR 99 after 128 h exposure at 800 °C in air.

outward diffusion of nickel on alloys MAR M 002 and SRR 99. Based upon the results obtained, it could be concluded that the coating maintained its stability during exposure at 800 °C. However, it became structurally unstable as a result of exposure at 1000 and 1100 °C. During exposure at 1000 °C, the structure of the outer coating layer changed from a mixture of $PtAl_2$ and NiAl into a mixture of NiAl and Ni_3Al. As a result of exposure at 1100 °C, the outer coating layer consisted only of Ni_3Al. Also, at both temperatures, the composition of the outer coating layer approached that of the inner layer due to interdiffusion. Although the structural stability of the coating on each alloy was similar, the coating on alloy MAR M 002 developed a more protective scale in comparison with that on alloy SRR 99. This behaviour could be attributed to differences in alloy substrate composition, particularly the presence of hafnium in alloy MAR M 002 and its absence in alloy SRR 99.

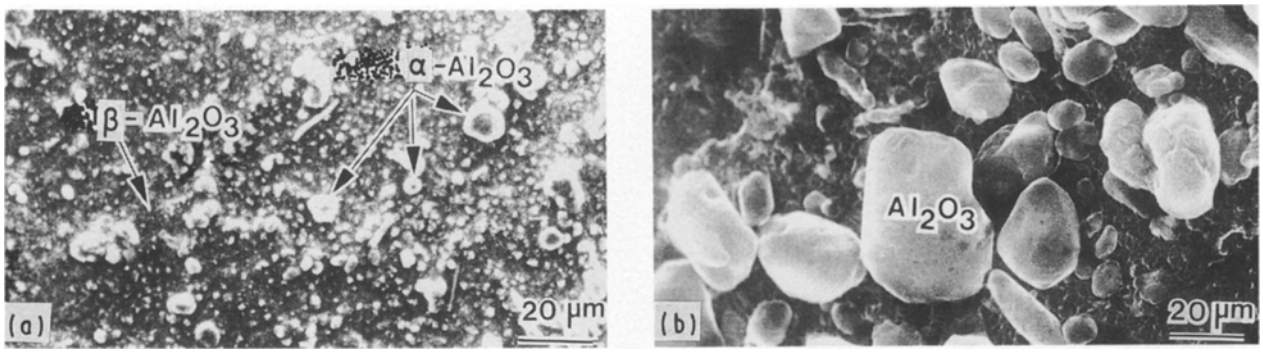

Figure 19 Secondary electron SEM images illustrating the morphology of surface scale developed by the coating on alloys (a) MAR M 002 and (b) SRR 99 after 500 h exposure at 1000 °C in air.

Acknowledgement

We thank Rolls-Royce plc, for financial support and for providing the coated alloys used in this study. The support of the Research Institute, King Fahd University of Petroleum and Minerals, where this study was carried out, is greatly appreciated.

References

1. J. H. WOOD and E. H. GOLDMAN, in "Superalloys II", edited by C. T. Sims, N. S. Stoloff and W. C. Hagel (Wiley, New York, 1987) p. 359.
2. P. C. PATNAIK, *Mater. Manufact. Process.* **4** (1989) 133.
3. R. STREIFF and D. H. BOONE, *J. Mater. Engng* **10** (1988) 15.
4. J. S. SMITH and D. H. BOONE, in "35th ASME International Gas Turbine Conference", Brussels, Belgium, Paper no. 90-GT-319, (ASME, New York, 1990).
5. H. M. TAWANCY, N. M. ABBAS and T. N. RHYS-JONES, *Surface and Coatings Technology* **49** (1991) 7.
6. J. SCHAEFFER, G. M. KIM, G. H. MEIER and F. S. PETTIT, in "The Role of Active Elements in the Oxidation Behaviour of High Temperature Metals and Alloys", edited by E. Lang (Elsevier Applied Science, London, New York, 1989) p. 231.
7. M. R. JACKSON and J. R. RAIRDEN, *Met. Trans.* **8A** (1977) 697.
8. N. BIRKS, G. H. MEIER and F. S. PETTIT, in "Superalloys, Supercomposites and Superceramics", edited by J. K. Tien and T. Caulfield (Academic Press, New York, 1989) p. 439.
9. F. S. PETTIT and C. S. GIGGINS, in "Superalloys II", edited by C. T. Sims, N. S. Stoloff and W. C. Hagel (Wiley, New York, 1987) p. 327.
10. G. W. GOWARD, *J. Metals* **22**(10) (1970) 31.
11. J. L. SMIALEK and C. E. LOWELL, *J. Electrochem. Soc.* **121** (1974) 800.
12. O. MOROCUTTI (ed.), "A Guide to the Control of High Temperature Corrosion and Protection of Gas Turbine Materials" (Commission of the European Communities, Brussels, Belgium, 1986) p. 50.
13. W. J. MOLLOY, *Adv. Mater. Process.* **138**(10) (1990) 23.
14. R. L. DRESHFIELD, *J. Metals* **39**(7) (1987) 16.
15. G. BERANGER, F. A. ARMANET and M. LAMBERTIN, in "The Role of Active Elements in the Oxidation Behaviour of High Temperature Metals and Alloys", edited by E. Lang (Elsevier Applied Science, London, New York, 1989) p. 33.
16. H. M. TAWANCY, *Met. Trans.* **22A** (1991) 1463.

Received 2 September 1991
and accepted 16 January 1992